

Probing IGM Physics during Cosmic Dawn using the Redshifted 21-cm Bispectrum

Mohd Kamran^{1, a}, Suman Majumdar^{1,2}, Raghunath Ghara^{3,4}, Garrelt Mellema⁵,
Somnath Bharadwaj⁶, Jonathan R. Pritchard², Rajesh Mondal⁵, and Ilian T. Iliev⁷

¹Department of Astronomy, Astrophysics & Space Engineering,
Indian Institute of Technology Indore, Indore 453552, India

²Department of Physics, Blackett Laboratory, Imperial College, London SW7 2AZ, U. K.

³ARCO (Astrophysics Research Center), Department of Natural Sciences,
The Open University of Israel, 1 University Road, PO Box 808, Ra'anana 4353701, Israel

⁴Department of Physics, Technion, Haifa 32000, Israel

⁵The Oskar Klein Centre and The Department of Astronomy,
Stockholm University, AlbaNova, SE-10691 Stockholm, Sweden

⁶Department of Physics, Indian Institute of Technology Kharagpur, Kharagpur - 721302, India and

⁷Department of Physics and Astronomy, Pevensey II Building, University of Sussex, Brighton BN1 9QH, UK

With the advent of the first luminous sources at Cosmic Dawn (CD), the redshifted 21-cm signal, from the neutral hydrogen in the Inter-Galactic Medium (IGM), is predicted to undergo a transition from absorption to emission against the CMB. Using simulations, we show that the redshift evolution of the sign and the magnitude of the 21-cm bispectrum can disentangle the contributions from Ly α coupling and X-ray heating of the IGM, the two most dominant processes which drive this transition. This opens a new avenue to probe the first luminous sources and the IGM physics at CD.

Introduction.— The Cosmic Dawn (CD) and Epoch of Reionization (EoR) are the periods in the history of the Universe during which the formation of the first sources of radiation caused major changes in the thermal and ionization states of the Inter-Galactic Medium (IGM). Various complex astrophysical processes dictate the state of the IGM during CD [1, 2].

The redshifted 21-cm line, originating from the hyperfine spin-flip transition of the electron in the ground state of neutral hydrogen atoms (HI), can trace the cosmological and astrophysical evolution of the IGM during CD in the most direct manner. Ongoing and upcoming radio interferometric experiments e.g. GMRT [3], LOFAR [4], MWA [5], PAPER [6], HERA [7] and SKA [8] are expected to be sensitive enough to probe this signal from the CD through various statistics such as the variance [9, 10], power spectrum [11], etc.

The power spectrum measures the amplitude of fluctuations in a signal at different length scales and can fully quantify the statistical properties of a pure Gaussian random field. However, the CD 21-cm signal is highly non-Gaussian due to the joint effects of the non-random distribution of first light sources in the IGM, the nature of the radiation emitted by these sources, as well as the interaction of this radiation with the HI gas in the IGM [12–14]. The nature and strength of fluctuations of this signal at any location in the IGM are determined by the relative population densities of the two different spin states of the 1s ground state of the HI atom. This ratio is commonly expressed as $n_1/n_0 = 3 \exp(-0.068 \text{ K}/T_S)$, where T_S is the so-called spin temperature, n_1 and n_0 are the population densities of the parallel and antiparallel spin states respectively. Different IGM processes, determined by the nature of the different types of radiation coming from the first sources, affect this ratio. Thus, the fluctuations in the HI 21-cm signal are expected to carry the signatures of these IGM processes [1]. In other words, the nature of the fluctuations in the signal and therefore its inherent

non-Gaussianity is determined by which IGM process dominates at what cosmic time [12, 15–19]. The power spectrum is not sensitive to this non-Gaussianity in the signal, hence one cannot probe the IGM physics solely based on this statistic. Higher-order statistics such as the bispectrum are required to describe how the 21-cm signal's non-Gaussianity evolves at different length scales [15–21].

Compared to the power spectrum, which is always positive by definition, the CD 21-cm bispectrum can be either positive or negative [15–19]. We thus expect the sign and magnitude of the bispectrum to be dependent on the dominant IGM processes, as these processes dictate the nature of non-Gaussianity in the signal. It is therefore imperative to ask whether the sign and magnitude evolution of the 21-cm bispectrum can identify which IGM processes dominate at which stage of the CD.

In this letter we demonstrate for the first time that it is possible to probe the CD IGM physics through the evolution of the sign and magnitude of the 21-cm bispectrum.

Simulating the HI 21-cm signal from the Cosmic Dawn.— This work is based on an N-body simulation using the CUBEP³M code [22] in a volume $(500 h^{-1})^3$ comoving Mpc³ using 6912³ dark matter particles. The resolved halos have been identified with having at least 25 particles, resulting in minimum halo mass $\approx 10^9 M_\odot$. The dark matter density and velocity fields were interpolated on a 600³ grid. We then use these ingredient fields in the 1D radiative transfer code GRIZZLY [23, 24] to simulate the 21-cm differential brightness temperature (δT_b) maps at 22 redshift snapshots in the range $z = 9$ to 20 following the equations in [1]:

$$\delta T_b(\mathbf{r}, z) = 27 x_{\text{HI}}(\mathbf{r}, z) (1 + \delta_b(\mathbf{r}, z)) \left(1 - \frac{T_{\text{CMB}}(z)}{T_S(\mathbf{r}, z)} \right) \times \left(\frac{\Omega_b h^2}{0.023} \right) \left(\frac{0.15}{\Omega_m h^2} \frac{1+z}{10} \right)^{1/2} \text{ mK} \quad (1)$$

where \mathbf{r} is the comoving distance to the source of emission,

Processes \ Scenarios	Model-a ₀	Model-a	Model-b	Model-c
Ly α -coupling	Yes	Yes	Saturated	Yes
X-ray heating	No	No	Yes	Yes
Ionization	No	Yes	Yes	Yes

TABLE I. All simulated CD scenarios considered in this study.

z is the redshift at which the signal was emitted, $x_{\text{HI}}(\mathbf{r}, z)$ is the hydrogen neutral fraction, $\delta_b(\mathbf{r}, z)$ is the fluctuations in the underlying baryon density and $T_{\text{CMB}}(z)$ is the Cosmic Microwave Background (CMB) radiation temperature. The spin temperature is connected to the IGM processes via the equation

$$T_S(\mathbf{r}, z) = \frac{T_{\text{CMB}}(z) + x_\alpha(\mathbf{r}, z)T_g(\mathbf{r}, z)}{1 + x_\alpha(\mathbf{r}, z)} \quad (2)$$

Hence the value of T_S will be determined by the strength of the Ly α coupling process x_α and the temperature of the IGM, T_g . T_g is determined by the adiabatic cooling due to cosmological expansion and the heating due to X-ray sources. Here we do not consider the impact of collisions on T_S as our redshift range ($20 > z > 9$) is well below the regime where collisions are important ($z \gtrsim 30$) [1]. Hence, the evolution of the fluctuations in the 21-cm signal depends on the changes in the Ly α coupling, X-ray heating and photo-ionization of the IGM gas and below we will focus on the impact of these three processes on the bispectrum. The 21-cm signal will be observed in either absorption or emission depending on whether the factor $(1 - T_{\text{CMB}}/T_S)$ is negative or positive, respectively. However, once heating has raised T_g substantially above T_{CMB} at late stages of the CD, the 21-cm emission becomes insensitive to the value of T_S , a regime known as spin temperature saturation, and then photo-ionization becomes important.

Further, the X-ray sources in our simulations have a spectral energy density $I_X(E) \propto E^{-\alpha}$ with $\alpha = 1.5$ which roughly represents mini-QSOs [25, 26]. These are expected to be the major sources of the soft X-ray photons during the CD. Apart from the X-ray photons produced by mini-QSOs, we also consider the contributions from star forming galaxies which produce ionizing photons. We further assume the stellar content of a galaxy to be proportional to the mass of the dark matter halo that hosts the galaxy. Thus, the stellar mass inside a halo of mass M_{halo} is $M_\star = f_\star \left(\frac{\Omega_b}{\Omega_m} \right) M_{\text{halo}}$ where f_\star is the star formation efficiency. We choose $f_\star = 0.03$ [27, 28] throughout this paper. More details about these simulations can be found in [19].

We have applied the effect of the redshift space distortions (RSD) to these simulated δT_b cubes by using the MM-RRM scheme of [29]. The cosmological parameters used in the simulations are $h = 0.7$, $\Omega_m = 0.27$, $\Omega_\Lambda = 0.73$, $\Omega_b = 0.044$, which are consistent with *WMAP* [30] and *Planck* results [31].

In this letter we consider four different scenarios for the evolution of the signal from the Cosmic Dawn as listed in Table I. The first three are simplistic and extreme scenarios

in which only a single physical process dominates the fluctuations in the 21-cm signal. The fourth scenario includes all three physical processes and therefore is the most realistic CD scenario. We use the first three scenarios to demonstrate the unique signatures of each of the three physical processes on the 21-cm bispectrum, which eventually helps us in explaining the bispectrum from Model-c, the most realistic scenario. The details of these scenarios are as follows: In Model-a₀, we only consider the evolution of Ly α coupling in a cold and neutral IGM. Model-a is a modified version of Model-a₀ where we also include the effect of photo-ionization of HI in the IGM. In Model-b, we consider the processes of X-ray heating and ionization but assume that a very strong Ly α background fully couples T_S to T_g . Finally, in Model-c, we include all of these processes in a self-consistent manner. Figure 1 shows the slices through the δT_b cube from very early to very late stages of the CD (left to right) for Model-a (top panels), Model-b (middle panels), and Model-c (bottom panels). The redshift evolution of the $\delta \bar{T}_b$ (global signal) for all of these models are shown in the left panel of Figure 2.

Note that in this letter we are specifically interested to explore the impact of IGM physics on the bispectrum during CD, specifically when Ly α coupling and X-ray heating are the most dominant processes. However, we also wanted to include the later stages of the CD in our analysis, when it gradually transitions to the EoR, thus up to $\sim 10\%$ of HI ionization has been considered in our models.

Bispectrum estimation.— We adopt the bispectrum estimator and associated algorithm discussed in [15, 18] to compute the bispectrum from the simulated data as

$$\hat{B}_i(\mathbf{k}_1, \mathbf{k}_2, \mathbf{k}_3) = \frac{1}{N_{\text{tri}} V} \sum_{[\mathbf{k}_1 + \mathbf{k}_2 + \mathbf{k}_3 = 0] \in i} \Delta_{21}(\mathbf{k}_1) \Delta_{21}(\mathbf{k}_2) \Delta_{21}(\mathbf{k}_3), \quad (3)$$

where $\Delta_{21}(\mathbf{k})$ is the Fourier transform of $\delta T_b(\mathbf{r})$, V is the observation or simulation volume and N_{tri} is the number of closed triangles associated with the i^{th} triangle configuration bin while satisfying the condition $\mathbf{k}_1 + \mathbf{k}_2 + \mathbf{k}_3 = 0$. Throughout this letter, we discuss spherically averaged bispectrum estimates obtained from our simulations.

Results.— We estimate the power spectrum $[P(k)]$ and bispectrum $[B(k_1, k_2, k_3)]$ for all CD scenarios of Table I for $k_1 = 0.16 \text{ Mpc}^{-1}$, which represents large length scales that can be potentially probed by telescopes e.g. SKA. For the sake of convenience, we designate $k_1 \leq 0.16 \text{ Mpc}^{-1}$ as ‘large-scale’. We normalize these statistics as $\Delta^2(k) = k_1^3 P(k)/2\pi^2$ and $\Delta^3(k_1, k_2, k_3) = k_1^3 k_2^3 B(k_1, k_2, k_3)/(2\pi^2)^2$. Recent studies [15, 18, 19] suggest that among all k -triangles, the magnitude of the bispectrum is maximum for the squeezed limit k -triangles. One would therefore expect the bispectrum for this shape of k -triangle to have the maximum signal-to-noise ratio [32, 33] and thus to have the highest probability of detection in future SKA observations. In addition to this, the squeezed limit bispectrum for $k_1 = k_2 = 0.16 \text{ Mpc}^{-1} > k_3 \rightarrow 0$, provides the correlation between the signal fluctuations at large and very large length scales. Motivated by this we only consider the

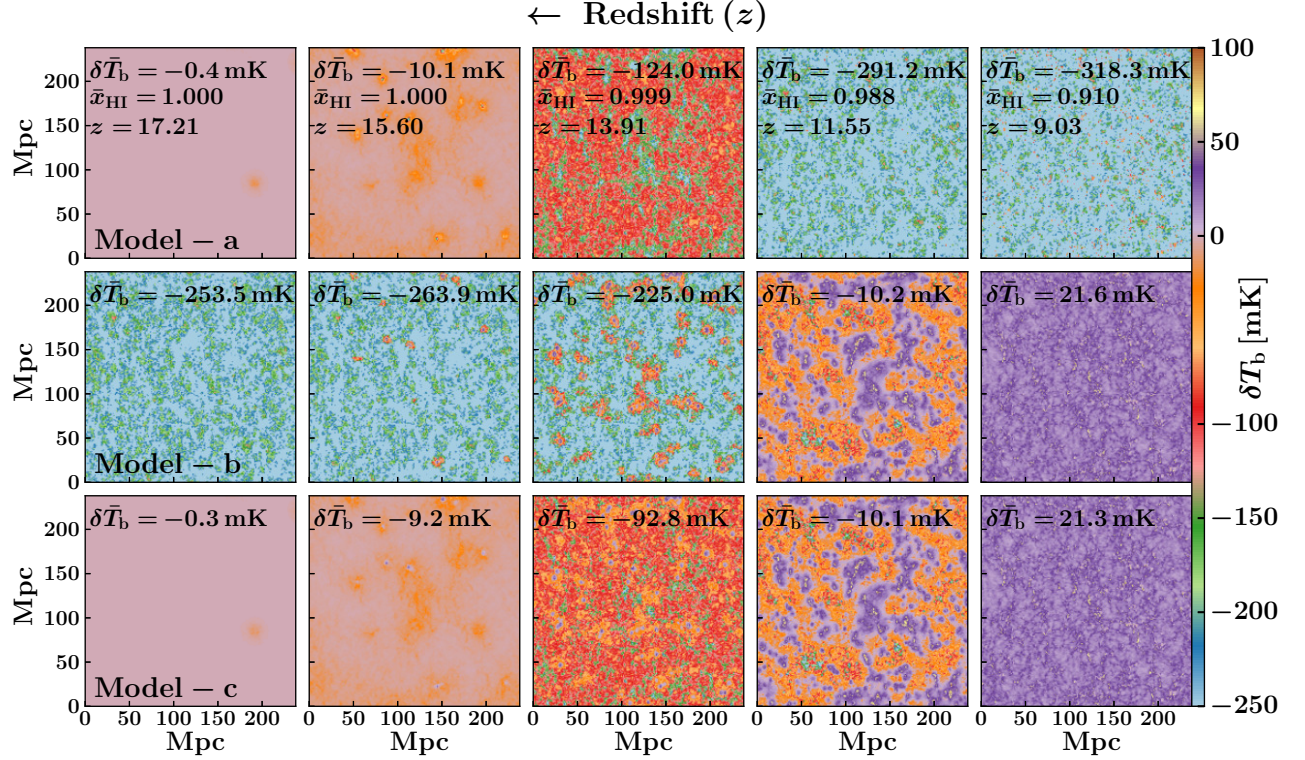


FIG. 1. Zoomed in slices (side length 238.09 Mpc) of the brightness temperature showing the redshift evolution of the 21-cm signal for scenarios Model-a (Top panels), Model-b (Middle panels), Model-c (Bottom panels). The full simulation volume is $(714.29 \text{ Mpc})^3$ in size.

large-scale squeezed limit bispectrum i.e. $[\Delta^3(k_1, k_2, k_3)]_{\text{Sq}}$ and investigate how they are affected by various IGM processes. The right panel in Figure 2 shows the redshift evolution of $[\Delta^3(k_1, k_2, k_3)]_{\text{Sq}}$. Note that we consider the k_1 bin width, $\Delta k_1 \sim 0.17 \text{ Mpc}^{-1}$, in such a manner that the centre of the bin corresponds to $k_1 \approx 0.16 \text{ Mpc}^{-1}$.

Before describing our results, we discuss the nature of the expected signal using simple analytical models. These will help us to interpret the basic nature of the results obtained from our simulations. Let us assume an IGM with uniform properties, and therefore uniform 21-cm signal (a ‘background’) in which one physical process locally changes the 21-cm signal around a source. For convenience, we also assume that the region with the changed 21-cm signal has a spherical shape. Such a description was used by [12, 15] for the case of a neutral, spin temperature saturated ($T_S \gg T_{\text{CMB}}$) background, which therefore has 21-cm in emission, in which photo-ionizing sources produce ionized regions with a zero 21-cm signal. They showed that the sign of the signal fluctuations of such a field in Fourier domain is negative and of the form: $\Delta_{21} \propto -W(kR) \sum \exp[i\mathbf{k} \cdot \mathbf{r}]$, where $W(kR)$ is the spherical top-hat window function, R is the comoving radius of the ionized spheres and the summation is performed over all such spheres with centres at \mathbf{r} . The negative sign is due to the regions having a lower signal than the background. The same approach can be used for other processes and backgrounds, for

example, a neutral heated (emission) region in a cold and neutral (absorption) background, which by analogy yields positive fluctuations.

Following this line of argument, one can predict the sign of the signal fluctuations on large-scales in scenarios when one of the three IGM processes is dominant. Note that we only consider the sign here, so the exact shape of the regions is irrelevant. The four relevant cases during CD are:

1. A Ly α coupled region in a neutral, cold and approximately uncoupled ($T_S \approx T_{\text{CMB}}$) background. The region will have a strong negative 21-cm signal in a very weak negative background. Consequently, the large-scale Δ_{21} will be negative.
2. An X-ray heated region ($T_S > T_{\text{CMB}}$) in a neutral, cold and fully Ly α coupled background ($T_S < T_{\text{CMB}}$). The region will have a positive 21-cm signal in a negative background. Consequently, the large-scale Δ_{21} will be positive.
3. An ionized region in a neutral, heated and fully Ly α coupled background ($T_S > T_{\text{CMB}}$). The region will have zero 21-cm signal in a positive background. Consequently, the large-scale Δ_{21} will be negative.
4. An ionized region in a neutral, cold and fully Ly α coupled background ($T_S < T_{\text{CMB}}$). The region will have

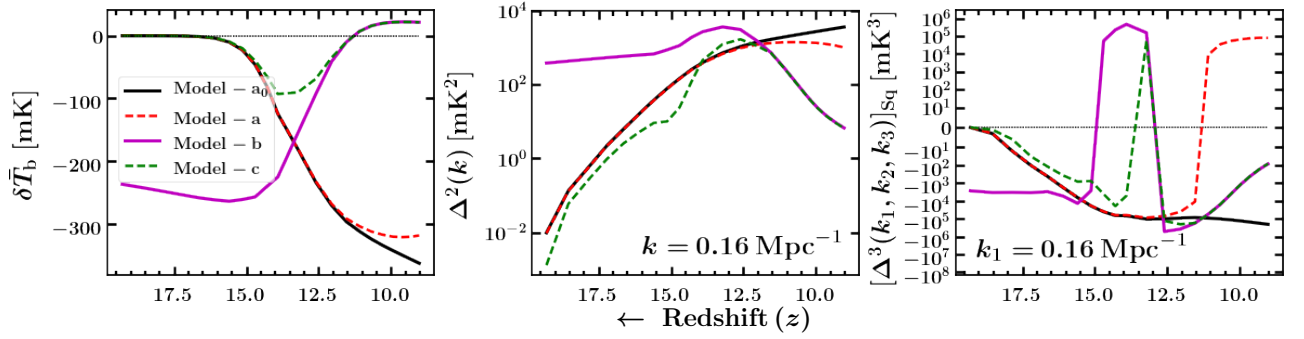


FIG. 2. Redshift evolution of the global 21-cm signal (left panel), the spherically averaged power spectrum at $k \sim 0.16 \text{ Mpc}^{-1}$ (middle panel), and the bispectrum for squeezed limit k -triangles with $k_1 \sim 0.16 \text{ Mpc}^{-1}$ (right panel). Different colours represent different CD scenarios as shown in Table I.

zero 21-cm signal in a negative background. Consequently, the large-scale Δ_{21} will be positive.

Bispectrum magnitude and sign.— As stated earlier, the large-scale squeezed limit bispectrum $[\Delta^3]_{\text{Sq}}$ probes the correlation between three large-scale Δ_{21} corresponding to the three k -modes of the squeezed limit k -triangle. Hence, one would expect the magnitude of $[\Delta^3]_{\text{Sq}}$ to depend on the magnitudes of these three Δ_{21} . Furthermore, the sign of $[\Delta^3]_{\text{Sq}}$ is given by the sign of the product of three Δ_{21} s averaged over the bin corresponding to the k -triangle. Hence, if the Δ_{21} s are positive, then $[\Delta^3]_{\text{Sq}}$ will be positive. Similarly, if the Δ_{21} s are negative, then $[\Delta^3]_{\text{Sq}}$ will be negative. We use this analogy only when we connect the simulated results to the simple analytical models.

Model- a_0 and Model- a .— The redshift evolution of the average or global signal $\delta\bar{T}_b$, the spherically averaged power spectrum Δ^2 and squeezed limit bispectrum $[\Delta^3]_{\text{Sq}}$ for Model- a_0 are shown by solid black lines in the left, middle and right panels of Figure 2. This CD scenario involves only the Ly α coupling process. This process starts with a negligible contribution to the global 21-cm signal during very early stages and gradually grows the 21-cm fluctuations with decreasing redshift (left panel of Figure 2). Due to this, the magnitude of the Δ_{21} gradually enhances and consequently causes the magnitude of $[\Delta^3]_{\text{Sq}}$ to increase with decreasing redshift. As expected from the analytical model 1, the sign of $[\Delta^3]_{\text{Sq}}$ is indeed negative.

For Model- a , $[\Delta^3]_{\text{Sq}}$ agrees with that for Model- a_0 until $z \sim 12$, as shown by the dashed red line in right panel of Figure 2. This is because the ionization process, which is included in Model- a but not in Model- a_0 , does not play a significant role until this redshift ($\bar{x}_{\text{HI}} \sim 0.99$). As ionization gains importance for $z \lesssim 12$, it causes a sign reversal in $[\Delta^3]_{\text{Sq}}$ from negative to positive. This is consistent with the expectation from the analytical model 4.

Model- b and Model- c .— Model- b , shown by magenta lines in Figure 2, considers X-ray heating in an IGM with fully saturated Ly α coupling ($T_{\text{S}} = T_{\text{g}}$). Hence, in this model, the 21-

cm signal transitions from a state of global absorption to a state of global emission. During the early stages ($19 \gtrsim z \gtrsim 15.5$), only a few X-ray sources are active. The heating they cause cannot compete with the adiabatic cooling due to the expansion of the Universe. The net effect is a gradual cooling of the IGM that further decreases the T_{S} , at a faster rate than the CMB temperature does (as $T_{\text{CMB}} \propto (1+z)$). This implies a gradual enhancement in $|1 - T_{\text{CMB}}/T_{\text{S}}|$ with time during these early stages, and with a negative sign as $T_{\text{S}} < T_{\text{CMB}}$. This results in the negative $\delta\bar{T}_b$ with a slowly evolving magnitude seen in the left panel of Figure 2. In this redshift range Δ_{21} cannot be predicted analytically but seems to follow a similar trend as the global signal as $[\Delta^3]_{\text{Sq}}$ is found to be negative with a slowly evolving magnitude.

IGM heating in Model- b becomes important at $z \sim 15.5$ and reduces the magnitude of the absorption signal around the sources by producing warm (or less cold) regions (second panel from left in the middle row of Figure 1). Additionally, it also produces small heated regions (where 21-cm signal is in emission) around the same sources. This effect continues as heating progresses and results in an overall reduction in the magnitude of Δ_{21} until $z \sim 15$. The magnitude of the bispectrum also follows this trend for $15.5 \gtrsim z \gtrsim 15$. As heating progresses further by $z \sim 14.5$, the heated regions grow in number and size. The 21-cm signal fluctuations thus can be thought of as being due to a few emission regions embedded in an absorption background. This is the case as predicted in analytical model 2. Hence, the large-scale Δ_{21} will be positive. This will result in a positive $[\Delta^3]_{\text{Sq}}$ (i.e. a sign reversal in $[\Delta^3]_{\text{Sq}}$). In the redshift range $14.5 \gtrsim z \gtrsim 13$, heated regions grow substantially and percolate. Thus, in this redshift range although the signal fluctuations and its bispectrum cannot be predicted analytically, the simulated $[\Delta^3]_{\text{Sq}}$ remains positive by $z \sim 13$.

As heating progresses the regions grow in number and size and this percolation process leads to more and more heated regions overlapping, ultimately resulting in a single large connected cluster of heated regions. This will also result towards a situation where the heated emission regions occupy a larger

volume in the IGM than the cold absorption ones. Hence, we gradually move towards the scenario where a few isolated cold absorbing regions are embedded in a hot emitting background. The Δ_{21} s thus follow the trend predicted by model 2. This results in a negative $[\Delta^3]_{\text{Sq}}$, another sign reversal in $[\Delta^3]_{\text{Sq}}$, which is indeed seen at $z \sim 12.5$. Due to the continued X-ray heating, the leftover absorption regions disappear (see the two right most panels in the second row of Figure 1) and hence the magnitude of Δ_{21} also goes down, which in turn gradually reduces the $[\Delta^3]_{\text{Sq}}$ magnitude towards the end of the CD.

The physical insights obtained from Models-a₀, a and b can now be used to understand the evolution of $[\Delta^3]_{\text{Sq}}$ for the realistic CD scenario, Model-c. In the redshift range $19 \gtrsim z \gtrsim 14$ $[\Delta^3]_{\text{Sq}}$ for Model-c, shown by the dashed green line in the right panel of Figure 2, shows similar trends in shape and sign as that of Models-a₀ and a. We see that initially Model-c follows Models-a₀ and a, implying that Ly α coupling to cold gas is the dominant process during these stages. The sign reversal seen around $z \approx 14$ is due to X-ray heating becoming the dominant process, which remains the case until the end of the simulation at $z = 9$, as we see that Model-c follows Model-b. One important point to note here is that during $19 \gtrsim z \gtrsim 11.5$, the magnitude of $[\Delta^3]_{\text{Sq}}$ for Model-c is smaller than that of the Models-a₀, a and b, simply because the Ly α coupling has not yet saturated in Model-c.

Bispectrum a better probe of IGM physics.— We compare the evolution of the signal bispectrum with that of the power spectrum (middle panel of Figure 2) in their ability to identify the dominant IGM processes during the CD. We have demonstrated that the bispectrum via its sign and sign changes can conclusively tell us which IGM process dominates Δ_{21} at what cosmic time. The redshift evolution of the power spectrum does show certain subtle features at the time of transition from the dominance of one physical process to the other. However, as this statistic is always positive, it is difficult to unequivocally identify these transitions on the basis of the power spectrum alone.

Detectability of the CD 21-cm bispectrum.— Recently, [33] have studied the detectability of the 21-cm bispectrum from the EoR. They have shown that even in the presence of system noise and cosmic variance, a $\geq 5\sigma$ detection of the squeezed limit bispectrum is possible with SKA for $k_1 \lesssim 0.8 \text{ Mpc}^{-1}$. Since the maximum amplitude of the large-scale squeezed limit 21-cm bispectrum from the CD is ~ 2 orders of magnitude larger than that from the EoR [19] we therefore expect that the large-scale squeezed limit 21-cm bispectrum from the CD would be detectable with the SKA observations. The full detectability prediction is beyond the scope of this letter. We plan to explore it in future.

Summary and conclusions.— In this letter we show for the first time how the two major IGM processes affecting the 21-cm signal during the CD, namely Ly α coupling and X-ray heating, impact the magnitude and sign of large scale ($k_1 \sim 0.16 \text{ Mpc}^{-1}$) squeezed limit 21-cm bispectrum. We demonstrate that the sign of the $[\Delta^3]_{\text{Sq}}$ is negative as long as

Ly α coupling is the dominant IGM process. We show that this conclusion holds even in the presence of X-ray heating. The $[\Delta^3]_{\text{Sq}}$ goes through a double sign change, around the time when X-ray heating becomes the most dominant IGM process. We have further demonstrated that these transitions cannot be conclusively probed by the power spectrum.

Our analysis suggests that $[\Delta^3]_{\text{Sq}}$ is a better statistic to put constraints on the dominating IGM processes during CD. This will become important in the context of the future 21-cm observations of CD with the SKA. Our analysis here is restricted only to the CD, when ionization never becomes the dominant process for the 21-cm fluctuations. In future, we plan to explore the connection of the sign of $[\Delta^3]_{\text{Sq}}$ with the IGM physics during the EoR.

Acknowledgements.— SM and GM are supported by the ASEM-DUO India 2020 fellowship. RG is supported by the Israel Science Foundation grant 255/18. GM is supported by Swedish Research Council grant 2020-04691. RM is supported by the Wenner-Gren Postdoctoral Fellowship. ITI is supported by Science and Technology Facilities Council (grants ST/I000976/1 and ST/T000473/1) and Southeast Physics Network (SEP-Net). Some of the numerical results (N-body simulations) were obtained via supercomputing time awarded by PRACE (Partnership for Advanced Computing in Europe) grants 2012061089, 2014102339, 2014102281 and 2015122822 under the project PRACE4LOFAR.

^a kamranmohd080@gmail.com

- [1] J. R. Pritchard and A. Loeb, *PRD* **78**, 103511 (2008).
- [2] J. R. Pritchard and A. Loeb, *Rep. Prog. Phys.* **75**, 086901 (2012).
- [3] G. Paciga, J. G. Albert, and et al., *MNRAS* **433**, 639 (2013).
- [4] F. G. Mertens, M. Mevius, and et al., *MNRAS* **493**, 1662 (2020).
- [5] N. Barry, M. Wilensky, and et al., *ApJ* **884**, 1 (2019).
- [6] M. Kolopanis, D. Jacobs, and et al., *ApJ* **883**, 133 (2019).
- [7] D. R. DeBoer, A. R. Parsons, and et al., *PAPS* **129**, 045001 (2017).
- [8] L. Koopmans, J. Pritchard, and et al., in *Advancing Astrophysics with the Square Kilometre Array (AASKA14)* (2015) p. 1.
- [9] I. T. Iliev, G. Mellema, and et al., *MNRAS* **384**, 863 (2008).
- [10] C. A. Watkinson and J. R. Pritchard, *MNRAS* **454**, 1416 (2015).
- [11] H. Jensen, K. K. Datta, and et al., *MNRAS* **435**, 460 (2013).
- [12] S. Bharadwaj and S. K. Pandey, *MNRAS* **358**, 968 (2005).
- [13] G. Mellema, I. T. Iliev, U.-L. Pen, and P. R. Shapiro, *MNRAS* **372**, 679 (2006).
- [14] R. Mondal, S. Bharadwaj, and et al., *MNRAS* **449**, L41 (2015).
- [15] S. Majumdar, J. R. Pritchard, R. Mondal, C. A. Watkinson, S. Bharadwaj, and G. Mellema, *MNRAS* **476**, 4007 (2018).
- [16] C. A. Watkinson, S. K. Giri, H. E. Ross, K. L. Dixon, I. T. Iliev, G. Mellema, and J. R. Pritchard, *MNRAS* **482**, 2653 (2019).
- [17] A. Hutter, C. A. Watkinson, J. Seiler, P. Dayal, M. Sinha, and D. J. Croton, *MNRAS* **492**, 653 (2020).
- [18] S. Majumdar, M. Kamran, J. R. Pritchard, and et al., *MNRAS* **499**, 5090 (2020).
- [19] M. Kamran, R. Ghara, S. Majumdar, and et al., *MNRAS* **502**, 3800 (2021).
- [20] S. K. Giri, A. D'Aloisio, G. Mellema, E. Komatsu, R. Ghara, and S. Majumdar, *J. Cosmology Astropart. Phys.* **2019**, 058 (2019).

- [21] Q.-B. Ma, B. Ciardi, M. B. Eide, and et al., *ApJ* **912**, 143 (2021).
- [22] J. Harnois-Déraps, U.-L. Pen, I. T. Iliev, H. Merz, J. D. Emerson, and V. Desjacques, *MNRAS* **436**, 540 (2013).
- [23] R. Ghara, G. Mellema, S. K. Giri, T. R. Choudhury, K. K. Datta, and S. Majumdar, *MNRAS* **476**, 1741 (2018).
- [24] R. Ghara, T. R. Choudhury, and K. K. Datta, *MNRAS* **447**, 1806 (2015).
- [25] S. Gallerani, L. Zappacosta, and et al., *MNRAS* **467**, 3590 (2017).
- [26] S. Martocchia, E. Piconcelli, and et al., *AAP* **608**, A51 (2017).
- [27] P. S. Behroozi and J. Silk, *ApJ* **799**, 32 (2015).
- [28] G. Sun and S. R. Furlanetto, *MNRAS* **460**, 417 (2016).
- [29] Y. Mao, P. R. Shapiro, G. Mellema, I. T. Iliev, J. Koda, and K. Ahn, *MNRAS* **422**, 926 (2012).
- [30] G. Hinshaw, D. Larson, E. Komatsu, and et al., *ApJS* **208**, 19 (2013).
- [31] Planck Collaboration, P. A. R. Ade, N. Aghanim, C. Armitage-Caplan, M. Arnaud, , and et al., *AAP* **571**, A16 (2014).
- [32] C. A. Watkinson, B. Greig, and A. Mesinger, *MNRAS* **510**, 3838 (2022).
- [33] R. Mondal, G. Mellema, A. K. Shaw, M. Kamran, and S. Majumdar, *MNRAS* **508**, 3848 (2021).